Journal of Electroceramics, 7, 47–56, 2001

Microstructural Design and Properties of $LaCoO_3/La_2(Zr,Y)_2O_{7-\delta}$ Composites

F.M. FIGUEIREDO,[1,2] F.M.B. MARQUES[2] & J.R. FRADE[2]

[1] *Science and Technology Department, Universidade Aberta, R. Escola Politécnica, 147 1269-001 Lisbon, Portugal*

[2] *Ceramics and Glass Engineering Department, UIMC, University of Aveiro 3810-193 Aveiro, Portugal*

Submitted January 19, 2001; Revised April 12, 2001; Accepted May 8, 2001

Abstract. $LaCoO_{3-\delta}/La_2(Zr,Y)_2O_7$-based composites were designed in view of three main properties: electrical conductivity, thermal expansion and resistance to thermal cycling. Composition and processing conditions were investigated on the basis of an experimental plan according to the Taguchi method. The phase distribution was estimated from image analysis and related to electrical and thermo-mechanical behavior. Results indicate that an homogeneous and fine grained phase distribution is essential in order to obtain materials with the desired thermal expansion, electrical properties and thermomechanical properties.

Keywords: composites, electrical conductivity, thermal expansion, $LaCoO_3$, Taguchi

1. Introduction

Fuel cells directly and continuously convert the chemical energy of a reaction between a fuel and an oxidant into electricity. In a Solid Oxide Fuel Cell (SOFC) a gaseous fuel (e.g. H_2) and an oxidant (oxygen) electrochemically react at high temperatures to produce electricity and heat. The basic cell consists of two porous electrodes separated by a gas tight oxygen-ion-conducting electrolyte. Yttria stabilized zirconia (YSZ) is the most common solid electrolyte, the cathode material is usually $La_{1-x}Sr_xMnO_{3-\delta}$ and the anode consists of a Ni/YSZ cermet [1].

Due to the high operation temperature of YSZ based SOFC's several constraints are placed on materials and on production technologies [2]. Alternative solid electrolytes like gadolinia-doped ceria (GCO) and Sr- and Mg-doped lanthanum gallate (LSGM) have thus been suggested for operation at lower temperatures due to a higher ionic conductivity and lower activation energy [2, 3]. Moving to lower operation temperatures also implies the need to improve electrode performance, and optimization of electrode microstructure and composition appears to be the solution [4].

It is known that $LaCoO_{3-\delta}$-based materials (LC) offer much better electrode performance than the standard $LaMnO_{3-\delta}$-based cathode materials (LM) [5]. Unfortunately, several problems hinder the use of these materials. Chemical instability results from excessive reaction with YSZ, forming a blocking layer of the pyrochlore $La_2Zr_2O_7$ (LZ) at the electrode/electrolyte interface [6, 7]. Also, thermal expansion mismatch between electrode and electrolyte seriously affects the mechanical integrity of the cell. The thermal expansion coefficient (TEC) of LC is close to $20 \times 10^{-6}\ K^{-1}$, which is approximately twice the value for YSZ and other solid electrolytes [1].

Lanthanum cobaltate remains relatively stable after firing in the presence of GCO and LSGM solid electrolytes [3], and has thus been the object of renewed interest and several attempts to overcome the thermal expansion mismatch, including partial replacement of La by Sr and/or of Co by Mn, Fe or Ni [8]. For example, a multi-layer composition gradient cathode, ranging from LC to LM [9] was suggested. LSFC with the general formula $La_{1-x}Sr_xFe_{1-y}Co_yO_{3-\delta}$ was also extensively studied [10, 11], including the chemical and thermal stability of the couple GCO/LSFC [12].

In this work, an attempt is made to lower the thermal expansion of LC-based cathodes by adding significant volume fractions of dispersed LZ with a relatively low thermal expansion ($TEC = 7 \times 10^{-6}\ K^{-1}$). The

experiments were conducted with a focus on the experimental design of these materials in order to characterize the influence of composition and phase distribution on the electrical and thermomechanical properties.

2. Experimental Procedures

2.1. Sample Preparation

$LaCoO_{3-\delta}/La_2(Zr_{0.84}Y_{0.16})_2O_7$/cobalt oxide three phase composites were prepared from mixtures of commercial powders of $LaCoO_{3-\delta}$ (Praxair Inc.) and yttria stabilized zirconia—YSZ ($(ZrO_2)_{0.92}(Y_2O_3)_{0.08}$ from Tosoh co.) according to the reaction [7]

$$2LaCoO_{3-\delta} + 2YSZ \Leftrightarrow La_2(Zr_{0.85}Y_{0.15})_2O_{7-\delta} + 2CoO + {}^1/_2O_2\nearrow \quad (1)$$

where the Y^{3+} ions are located at Zr^{4+} positions of the pyrochlore [6]. Powders were mixed in polypropylene containers with polypropylene balls for different periods. These powder mixtures were then uniaxially pressed (100 MPa for 1 min) into disks. Samples with 1 to 2 cm in diameter and 2 to 3 mm thick were obtained after sintering at 1400°C for 2 hours, with heating/cooling rates of 4 K/min.

The density of the samples was measured by the Archimedes method and compared to the values predicted on the basis of the theoretical density and volume fraction of each of the composite components.

2.2. Experimental Design

The appropriate design of such materials implies, very often, a considerable number of experiments due to the large number of variables and their possible cross-effects on materials properties. Planning of experiments is thus a key factor in materials design. Our approach is based on a plan where 4 different factors can assume 3 different values. Such a model leads to a complete experimental plan consisting of $3^4 = 81$ experiments. This number is high and somewhat discouraging. We thus adopted a reduced plan proposed by Taguchi [13] in which only 9 experiments (table $L_9(3^4)$) are required to model our system.

The main factor is *composition*. Three different volume fractions of the conductive phase $LaCoO_{3-\delta}$ were considered: 17, 41 and 62%.

The relative grain size distribution of the conductive phase, as well as its phase distribution, is also likely to play an important role on the overall behavior of the composite material. For instance, the percolation limit of the conductive phase in graphite/polymer composites was reduced to 12 vol.% by the use of smaller grains of graphite [14]. In order to modify the grain size of the cobaltate phase, the initial powder was used in three different degrees of agglomeration resulting from different *precalcination temperatures*.

The *mixing time* has proven to have a marked influence on both powder reactivity and homogeneity of the mixture. Three significantly different levels of mixing were achieved during 1, 10 and 100 min.

Another factor of simple experimental control is the *sintering temperature* of the pellets. In the initial plan, the sintering temperature was set to 1000, 1200 and 1400°C.

However, in the course of experiments, two unexpected findings required changes in the plan:

- some samples were not conveniently sintered at the lowest temperatures (1000 and 1200°C). All the samples were thus sintered at 1400°C;
- the mixing time in experiment 9 was increased from 1 to 100 min in order to obtain a dense sample, suitable for characterization.

The reduced plan and the chosen experimental parameters are summarized in Table 1. Somewhat long names were chosen to denote the different processing conditions, helping the reader in the discussion of the results. The generic notation LC*mcnto* indicates the vol.% of LC (m), the calcination temperature ($n = 0$ for uncalcined, $n = 10$ for 1000°C and $n = 12$ for 1200°C) and the mixing time (o) (in minutes). Two samples of each material were made and characterized

Table 1. Plan of experiments showing the different processing conditions.

Material	% $LaCoO_{3-\delta}$	T_{cal} (°C)	t_{mix} (min)
LC15c0t1	15	without	1
LC15c10t10	15	1000	10
LC15c12t100	15	1200	100
LC41c0t100	41	without	100
LC41c10t1	41	1000	1
LC41c12t10	41	1200	10
LC62c0t10	62	without	10
LC62c10t100	62	1000	100
LC62c12t100	62	1200	100

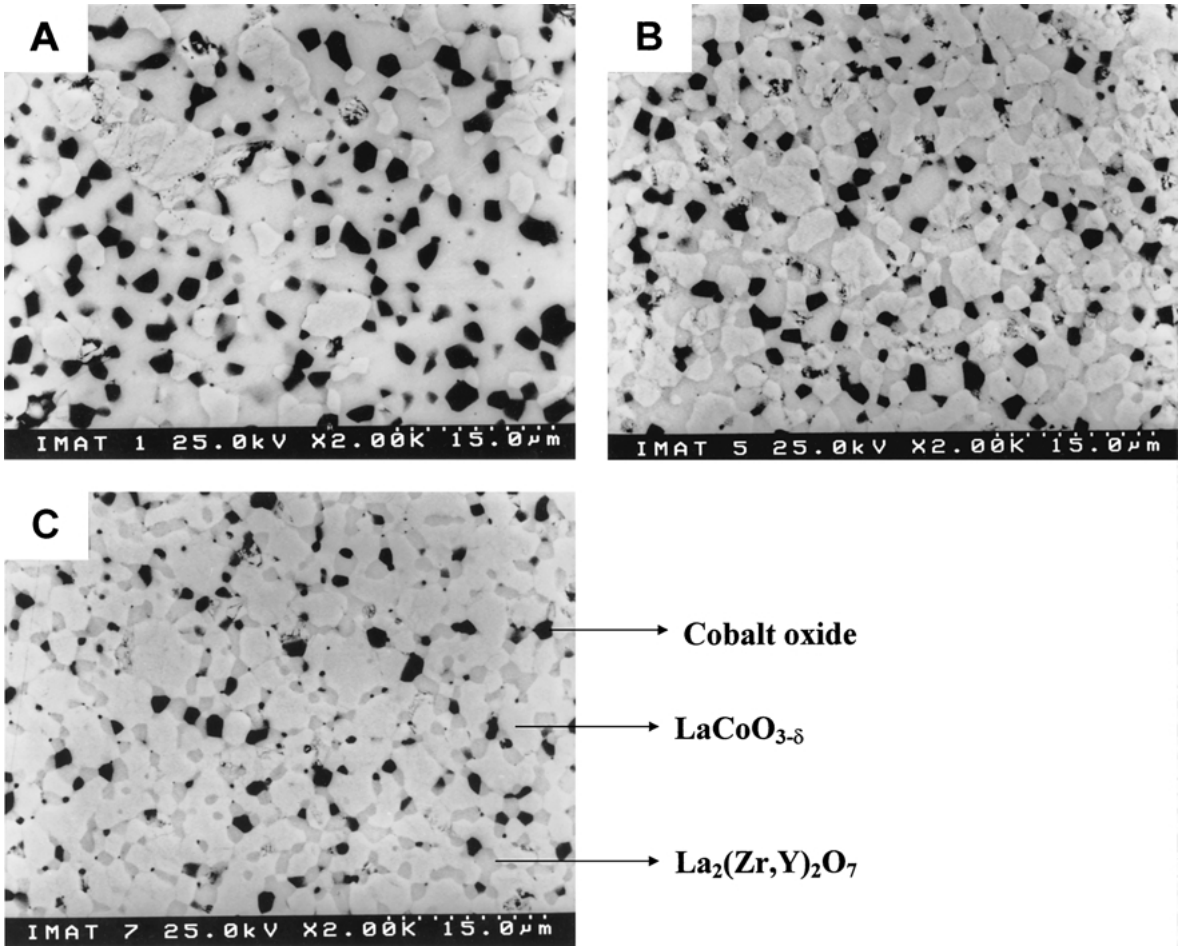

Fig. 1. SEM back-scattered micrographs of the composite materials. A, B and C correspond to the compositions with 17, 41 and 63 vol.% of $LaCoO_{3-\delta}$. The cobalt oxide is black, the cobaltate is the pale gray and the zirconate the darker gray.

in order to check for reproducibility. This was found to be satisfactory and the actual results are the average of the two samples.

2.3. Materials Characterization

Phase identification was carried out by XRD of fine powders obtained from grinding sintered pellets. The microstructures were characterized by optical microscopy (Leica) and SEM—scanning electron microscopy (Hitachi S4100). Micrographs were scanned (HP SCANJET 3P) and analyzed using the Leica Quantimet 500 QWIN v02.00 software package to evaluate the phase distribution.

In SEM back-scattered micrographs, the cobalt oxide is black and provides a clear picture of spatial distribution (Fig. 1). The zirconate appears light gray and the cobaltate is even lighter. Images obtained by optical microscopy were suitable to distinguish the relative amount of the cobalt-rich phases (cobaltate + cobalt oxide), with similar pale colors, from the darker lanthanum zirconate (Fig. 2). In both types of images, pores and cracks can be easily distinguished.

The homogeneity of the phase distribution in the composite materials was estimated through the distribution of the cobalt oxide. This reaction product is located at the cobaltate/zirconate interface and appears black in the back-scattered SEM micrographs, which is particularly suitable for image analysis.

Two factors are usually adopted to characterize the phase distribution in a given material [15]. Compositional differences found in different parts of

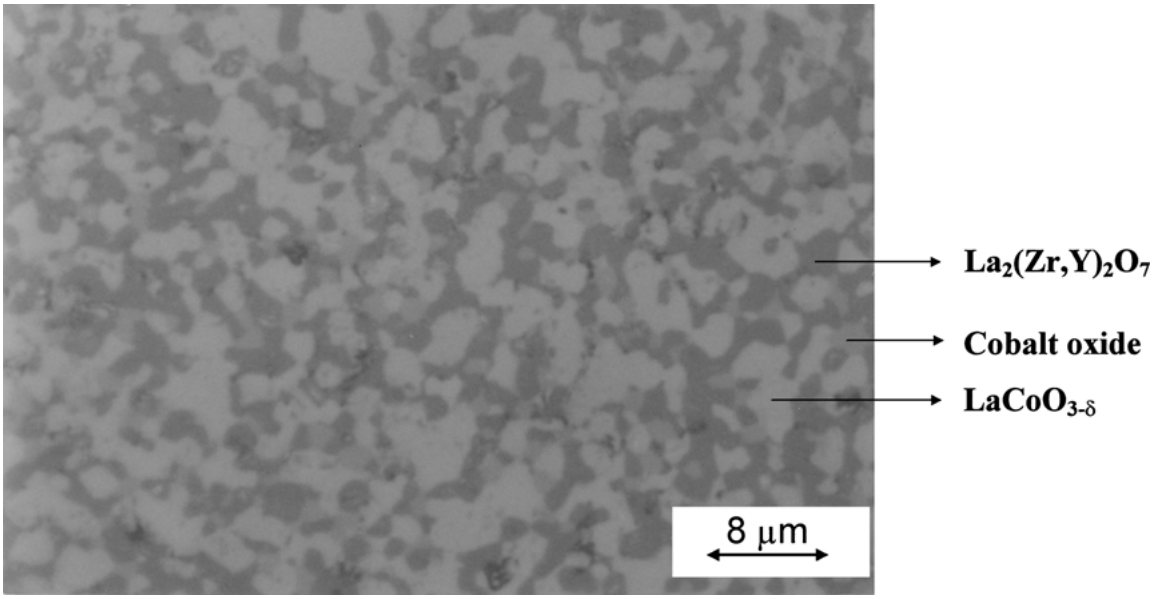

Fig. 2. Microstructure of a composite material (41 vol.% $LaCoO_{3-\delta}$) obtained by optical microscopy. The cobaltate and the cobalt oxide appear light gray, whilst the zirconate appears darker.

the material are interpreted in terms of the *intensity of segregation*. The intensity of segregation (IS) can be measured by a number that, in the case of our composite materials, could be the relative dispersion of the number of cobalt oxide grains per unit area $IS = (s/n_A) \times 100$, where n_A is the average number of grains per unit area and s the standard deviation.

A second parameter is needed to relate the intensity of segregation with the size of the sampling area, that is, a *scale of segregation*. This was obtained on comparing the intensity of segregation of the cobalt oxide grains found in increasingly large sampling areas.

The general procedure for the determination of the intensity and scale of segregation can be summarized as follows:

i) to obtain micrographs of 700 times linear magnification from 10 random positions on polished pellets;
ii) to perform digital image analysis to estimate the number of cobalt oxide grains in six areas of different size: 17708, 8369, 4170, 2010, 1072 and 495 μm^2. In order to ensure significant confidence levels, the number of different areas measured ranged from 10, for the largest area, to 240 for the smaller.
iii) to perform statistical analysis of the data to estimate the average number of grains per unit area (n_A) and the standard deviation (s).

Further details on the use of image analysis for microstructural studies can be found in the book by Coster and Chermant [16].

Thermal expansion coefficients were evaluated between room temperature and 950°C with heating/cooling rates of 5 K/min. The electrical conductivity (σ) was measured as a function of temperature with a modified dc van der Pauw method [17].

3. Phase Composition and Distribution

The XRD patterns shown in Fig. 3 qualitatively confirm the presence of the expected phases ($LaCoO_{3-\delta}$, $La_2(Zr,Y)_2O_7$ and cobalt oxide).

The analysis of the microstructures was used to check the composition of these materials. Table 2 shows results obtained with three homogeneous materials. These values are in reasonable agreement with the theoretical values predicted from reaction 1. Differences are probably due to partial oxidation of CoO to Co_3O_4 [18], and also because the experimental value is obtained from cross sections and the theoretical one is relative to a volume. The limited sampling areas, the

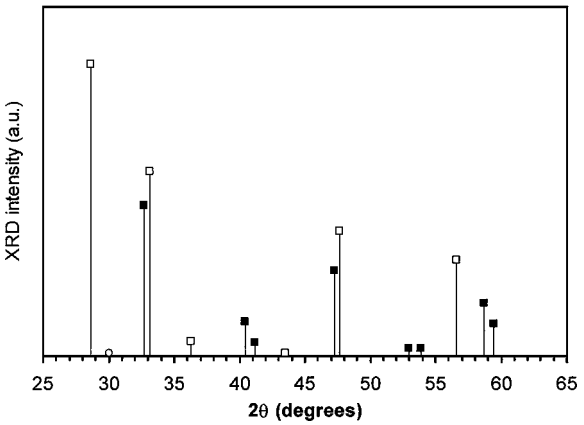

Fig. 3. XRD patterns of a composite with 41 vol.% cobaltate sintered at 1400°C for 2 h. Characteristic peaks from $LaCoO_{3-\delta}$ (■), $La_2(Zr_{0.84}Y_{0.16})_2O_7$ (□) and cobalt oxide Co_3O_4 (○).

existence of systematic errors in image scan and treatment may also contribute to such small deviations.

Table 3 shows the first series of results according to the previously introduced experimental plan, including the values of densification. In materials with cobaltate precalcined at 1200°C (LC15c12t100 and LC62c12t100), high mixing times are needed to obtain the highest densification. Comparison between these two materials suggests some influence of the cobaltate phase content. However, the effects of precalcination and mixing time also reveal that agglomerates affect the densification; this may also be affected by the release of O_2 during reaction (Eq. (1)) [19]. The results referring to LC41c0t100, LC41c10t1 and LC62c12t100 also show that agglomerates affect the densification.

Thermogravimetric analysis of the powder mixtures suggests the onset of the reaction at about 800°C [19]. Therefore, the consolidation of such reactive electrodes is expected to occur at lower temperatures than in single-phase materials.

The intensity of segregation (IS) of the phase distribution was evaluated through the distribution of cobalt oxide in sampling areas (A) with different sizes (Fig. 4). The figure shows that above 7500 μm^2 the parameter IS remains nearly independent of A. Results for samples of similar compositions in the low area range show the importance of the mixing time (see, for example samples LC62c0t10 and LC62c10t100). In the material LC62c0t10, the relatively high value of IS (≈15%) for

Table 2. Phase composition determined from image analysis. Values predicted according to reaction 1 are shown inside brackets.

		Material		
Technique	Phase	LC15c10t10	LC41c0t100	LC62c10t100
Optical microscopy	$LaCoO_3$ + Co oxide	31 (32)	49 (52)	70 (70)
SEM	$La_2(Zr,Y)_2O_7$	69 (68)	51 (48)	30 (30)
	Co oxide	16 (17)	8 (12)	5 (8)

Table 3. Densification (%D), thermal expansion coefficient (TEC) and total electrical conductivity (σ) at different temperatures of the composite materials.

		TEC × 10^6 (K^{-1})			
Material	%D	Low T	High T	$\sigma_{600°C}$ (S/m)	$\sigma_{800°C}$ (S/m)
LC15c0t1	95,5	10.0	10.0	780	3020
LC15c10t10	98,1	11.0	–	60	820
LC15c12t100	95,1	11.1	19.0	30	330
LC41c0t100	99,0	14.2	–	2610	8130
LC41c10t1	95,0	10,5	12,5	250	1750
LC41c12t10	86,8	10,1	13.1	220	1340
LC62c0t10	94,5	13.0	15.1	7980	20180
LC62c10t100	99,1	18,5	–	36970	43200
LC62c12t100	98,2	18,1	–	19170	25710

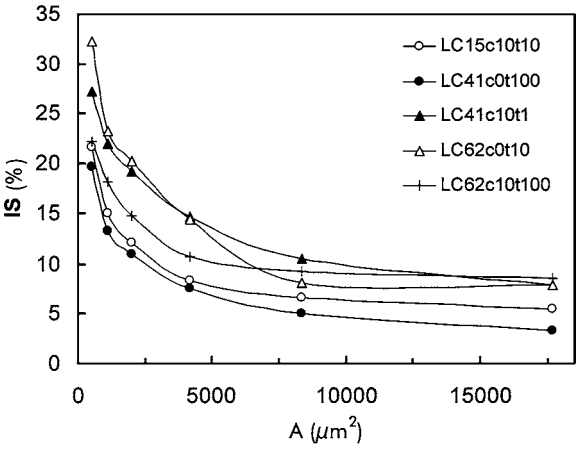

Fig. 4. Intensity of segregation versus scale of segregation associated to the cobalt oxide distribution in the three phase composites.

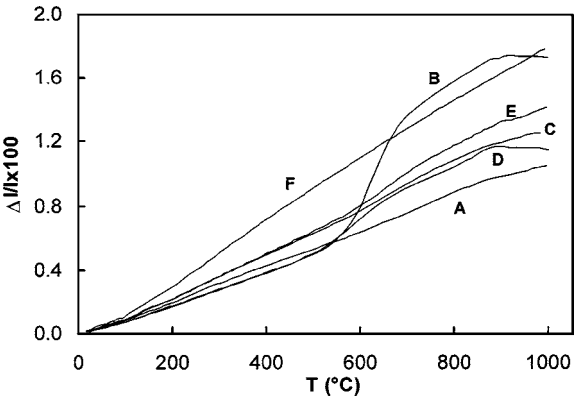

Fig. 5. Thermal expansion of several composite materials. A-LC15c10t10, B-LC15c12t100, C-LC41c0t100, D-LC41c0t1, E-LC62c0t10, and F-LC62c10t100.

A $< 5000\ \mu m^2$ resulted from a relatively short mixing time (10 min). On the other hand, the increase in mixing time to 100 min (sample LC62c10t100) was enough to decrease IS to $\approx 11\%$. Even greater differences can be seen for samples LC41c0t100 and LC41c10t1.

The surface area of single cobalt oxide grains showed little dependence on the processing conditions, with average values of 2 to 4 μm^2 estimated from equivalent grain diameter measurements. These values are more than three orders of magnitude lower than the limit defined by a typical scale of segregation ($A = 7500\ \mu m^2$).

In general, fine-grained reactants promote the reactivity and sinterability, as expected, and together with long mixing times decrease the intensity of segregation of the phase distribution. The existence of $LaCoO_3$ agglomerates in the initial mixture leads to increasing segregation of cobaltate and zirconate.

4. Thermal Expansion

Figure 5 shows the thermal expansion of triple phase composites. Some of these materials show a deviation from linear behavior with a sharp transition in the range 600 to 700°C. This change is more pronounced in LC15c12t100 with an unexpected increase of about 0.9% between 600°C to 750°C. A similar behavior can be identified more or less clearly in samples LC41c10t1 and LC62c0t10. Nearly linear behavior is observed for LC62c10t100 and pure cobaltate while LC15c10t10 and LC41c0t100 samples still show a slight transition.

The thermal expansion behavior of the composites is strongly dependent on the amount of the low thermal expansion phase (LZ) and on the existence of agglomerates of the high thermal expansion phase (LC). The influence of LC agglomerates can be verified comparing the results obtained for samples LC62c0t10 and LC62c10t100 (with 62% LC), LC41c0t100 and LC41c10t1 (with 41% LC), LC15c10t10 and LC15c12t100 (with 15% LC). The transition zone is sharper when LC was precalcined at relatively high temperatures and where low mixing times were used because these conditions are most likely to yield agglomerates (LC15c12t100, LC41c10t1 and LC62c0t10). The estimated TEC for the different materials and the differences between the low and high temperature ranges are shown in Table 3.

This behavior can be explained by the difficulty of the zirconate/cobalt oxide matrix in accommodating the excessive thermal expansion of cobaltate agglomerates. Note that the TEC of lanthanum zirconate is approximately three times smaller than for the perovskite.

The presence of separate phases originates two different thermal expansion regimes. At low temperature, the overall behavior is controlled by the zirconate, especially for materials with the highest volume fractions of this phase. However, the composite may be unable to accommodate the expansion of the cobaltate skeleton at higher temperatures, thus affecting the overall behavior. Evidence for this can be found in the thermal expansion curve of the LC15c12t100 material (Fig. 5—curve b). The TEC in the low

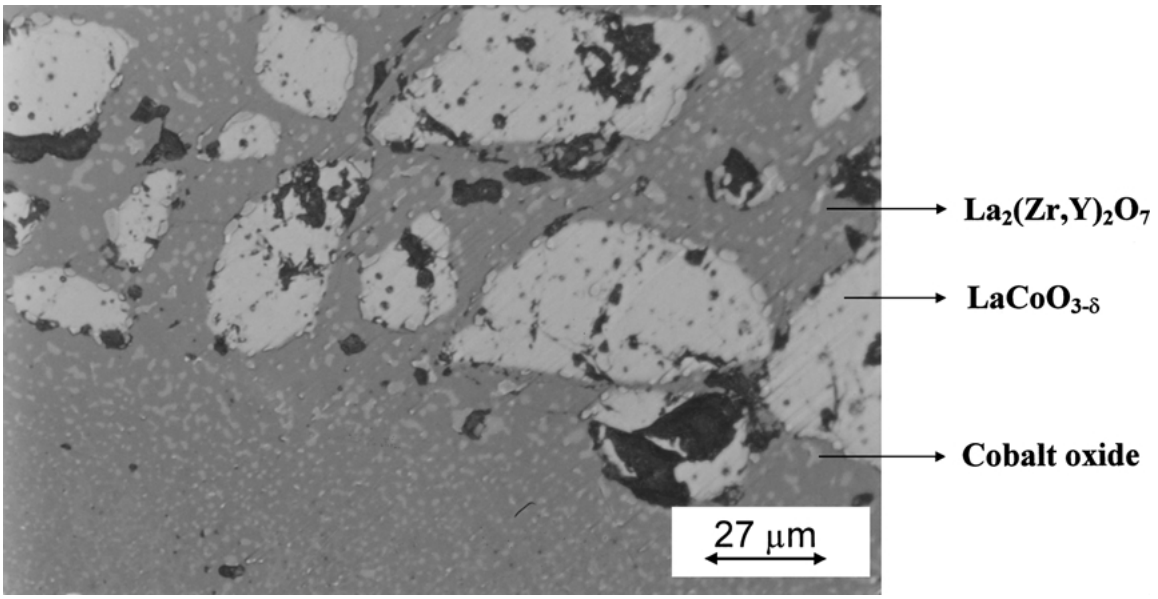

Fig. 6. Micrograph of the LC15c12t100 composite materials obtained by optical microscopy. The black areas are pores and cracks.

temperature regime is close to other composites with the same composition while in the high temperature regime the TEC approaches the value found for the cobaltate (see Table 3).

The microstructure of this material (Fig. 6) clearly shows phase segregation with large $LaCoO_3$ isolated agglomerates surrounded by the zirconate. This figure shows cracks along the interface, which may result from the thermal expansion mismatch between the $LaCoO_3$ agglomerates and the zirconate as well as from O_2 release. The stresses developed may even cause the collapse of the structure as suggested by the sharp decrease in the final part of the thermal expansion curves. This behavior can also be observed in the LC41c10t1 material, which has a different composition, but processed in similar conditions.

The control of the homogeneity of phase distribution is thus a critical feature in the design of composites with a macroscopically stable thermomechanical behavior.

5. Electrical Conductivity

The electrical conductivity of the triple phase composites was measured at different temperatures and typical results are presented in Table 3. In general, the conductivity strongly increases with increasing t_{mix}; likewise, decreasing T_{calc} decreases conductivity but to a lesser extent. For compositions with 15 vol.% of cobaltate, the conductivity varies over one order of magnitude with the processing conditions. As the cobaltate content diminishes the relative differences tend to increase, probably because heterogeneities disturb the percolation.

The more conductive compositions are less sensitive to the processing conditions. In this case the number of available paths for charge transport is high and, therefore, the percolation threshold is less likely to be affected by the processing conditions. The amount of reaction products also determines the overall behavior. The microstructural analysis has shown that the thermal expansion mismatch and the O_2 release from the reaction $LaCoO_3$ + YSZ leads to the formation of cracks in the material. These cracks will act as blocking elements lowering the connectivity of the conductive phase. It is thus obvious that highly homogeneous small-grained phase distribution is needed to enhance percolation and to avoid blocking effects.

The difference between conductivity measurements at 800°C and 600°C is also much higher for compositions with greater intensity of segregation, probably because blocking elements such as cracks are somewhat short-circuited by the expansion of the highly conductive regions. Note that the differences between $\sigma_{800°C}$

and $\sigma_{600^\circ C}$ are greater in composites with greater thermal expansion anomaly.

6. The Taguchi Approach

The traditional method for the investigation of multivariable processes is based on a separate study of effects while the others are kept constant [22]. When the number of parameters and parameter settings is high, the factorial plan will necessarily include a large number of experiments. To overcome this time consuming problem, alternative techniques were developed known as partial factorial experimental programs. These were first used in the mid twenties and have been used since the sixties by the Japanese industry, followed in the late seventies by American companies [14]. Although traditionally used in industry, some examples can also be found of the application of fractional experimental design in academic work [23, 24].

Among the existing methods, the Taguchi approach is particularly attractive for simplicity and clarity of use. The Taguchi partial plans are derived from predefined complete factorial plans, demanding from the experimentalist an effort of adaptation of the real problem to one of the existing simplified models proposed by Taguchi.

In a partial factorial plan, each parameter setting is associated to the same number of settings of each one of the other parameters—the orthogonal condition. This ensures a uniform coverage of the complete factorial plan and that each factor has an equal contribution to the plan. Taguchi proposed the analysis of data in terms of a signal to noise ratio and the existence of a loss function.

We retain in this work a very simplified analysis in terms of the effects of each factor in some properties of the composites such as densification, electrical conductivity and thermal expansion.

The results shown in Table 3 can be used to estimate the effect of each parameter on the different properties of the composites. For example, the effect of the mixing time set to 10 min corresponds to the difference between the partial average conductivity of the samples obtained with $t_{mix} = 10$ min and the total average conductivity ($\bar{\sigma}$):

$$\begin{aligned} E_{t_{mix}} &= 10 \text{ min} \\ &= \frac{\sigma_{LC15c10t10} + \sigma_{LC15c12t10} + \sigma_{LC15c0t10}}{3} - \bar{\sigma} \\ &= -4162. \end{aligned} \quad (2)$$

The same calculations can be extended to the effect of composition and calcination temperature and Eq. (2) generalized for any factor:

$$E_{fi=a} = M_{fi=a} - M \quad (3)$$

where $E_{fi=a}$ is the effect of factor fi set to a level a, $M_{fi=a}$ is the partial average response of the system when fi = a and M is the total average response of the system.

The calculated effects on densification (%D), electrical conductivity at 800°C ($\sigma_{800^\circ C}$) and the difference between the composite TEC and the goal value $TEC_{GCO} = 12.5 \times 10^{-6}$ K^{-1} ($TEC–TEC_{GCO}$) are shown in Fig. 7. The observed trends suggest that:

i. increasing the cobaltate content results in the increase of conductivity and thermal expansion.
ii. the increase in T_{calc} decreases densification and conductivity while the thermal expansion increases.
iii. increasing t_{mix} causes an increase in all properties.

These general trends are in good agreement with the discussion carried out in the previous sections. However, this simple approach may mislead the experimentalist by masking possible factor interactions. For example, the relatively low value found for $E_{\%D}$ in the materials with 41 vol.% cobaltate is due to a major contribution of one single material (LC41c12t10). This means that the level to which the factors are set can influence the effect of a given factor.

The main disadvantage of the Taguchi method is related to the fact that only a limited number of interactions between two factors can be analyzed. Interactions between n factors (nth order interaction, $n \geq 3$) are always considered negligible. The standard Taguchi tables can be divided in three groups: i) tables with no interactions, ii) tables that can handle one single interaction and, iii) tables in which some particular interactions can be allocated to one of the columns. Therefore, allocation of interactions in the Taguchi tables reduces the number of the studied parameters. In the chosen Taguchi plan, table $L_9(3^4)$, only the interaction between composition and precalcination temperature, the factors in the first two columns of the plan, is considered.

Interactions between factors can be estimated by:

$$I_{fi=a,fj=b} = \bar{M}_{fi=a,fj=b} - E_{fi=a} - E_{fj=b} - M \quad (4)$$

where $I_{fi=a,fj=b}$ is the interaction between factor fi = a and fj = b, $\bar{M}_{fi=a,fj=b}$ is the partial average response of the system when fi = a and fj = b. The interaction between composition and precalcination temperature

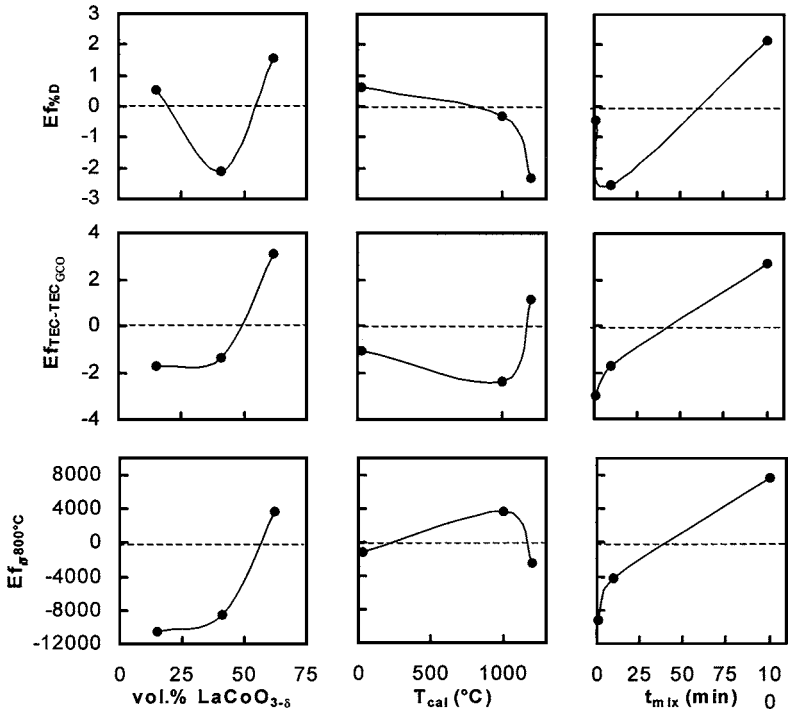

Fig. 7. Effect of composition, pre-calcination temperature and mixing time in $\sigma_{800^\circ C}$, %D and (TEC–TEC_{GCO}). The lines are a guide to the eye.

obtained with Eq. (4) is particularly significant when both factors are set to the maximum level (Fig. 8). This is an expected result since the number of agglomerates resulting from high precalcination temperatures is indeed higher in the samples with higher $LaCoO_{3-\delta}$ content.

Other expected interactions, such as the influence of the mixing time in the effect of the precalcination temperature, are completely neglected in our plan and confirming experiments are obviously needed. The L_9 table is thus clearly insufficient for a proper assessment of the interactions, but the information obtained with even such a simple model was precious for the development of the title materials reported elsewhere in greater detail [20].

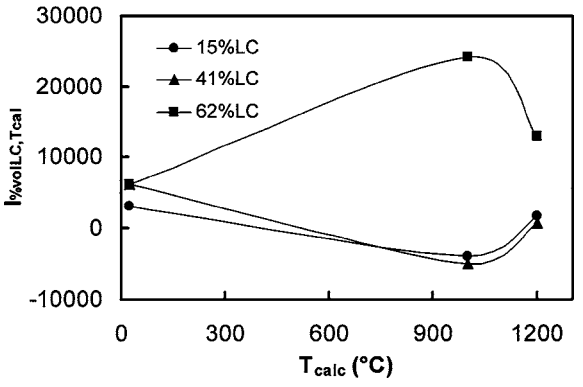

Fig. 8. Interaction between the $\sigma_{800^\circ C}$ effect of composition and pre-calcination temperature. The lines are a guide to the eye.

7. Conclusions

A high processing flexibility of $LaCoO_3$ + $La_2(Zr, Y)_2O_7$-based composites can be achieved by controlling parameters such as the mixing time or the initial grain size of the conducting phase. The homogeneity of the phase distribution proved to be critical for the thermomechanical stability and electrical properties of these materials. The existence of agglomerates leads to significant local stresses that may result in the formation of cracks and other discontinuities in the material. In this case, the electrical properties are severely compromised.

The Taguchi approach to fractional factorial experimental design can be an useful tool for the optimization

of the time effort of a given experimental task. A significant reduction of the number of experiments was achieved with a satisfactory level of knowledge on the system.

Acknowledgment

Financial support from Praxis XXI and FCT (Portugal) is greatly appreciated.

References

1. N.Q. Minh, *J. Amer. Ceram. Soc.*, **76**, 563 (1993).
2. K. Zheng, B.C.H. Steele, M. Sahibzada, and I.S. Metcalfe, *Solid State Ionics*, **86**, 1241 (1996).
3. K. Huang, M. Feng, J.B. Goodenough, and M. Schmerling, *J. Electrochem. Soc.*, **143**, 3630 (1996).
4. M. Kleitz and F. Petitbon, *Solid State Ionics*, **92**, 65 (1996).
5. Y. Ohno, S. Nagata, and H. Sato, *Solid State Ionics*, **3**, 439 (1981).
6. J.A. Labrincha, J.R. Frade, and F.M.B. Marques, *J. Materials Science*, **28**, 3809 (1993).
7. H. Yokokawa, N. Sakai, and T. Kawada, *J. Electrochem. Soc.*, **138**, 2719 (1991).
8. J. Mizusaki, M. Yoshiro, S. Yamauchi, and K. Fueki, *J. Electrochem. Soc.*, **136**, 2082 (1989).
9. E. Ivers-Tiffée, B. Jobst, I. Kraus, R. Schachtner, and M. Schiessl, *Proc. 2nd Int. Symp. on SOFC's (Addendum)*, edited by F. Gross, P. Zegers, S.C. Singhal, and O. Yamamoto (Commission of the European Communities, Luxembourg, 1991), p. 97.
10. L.W. Tai, M.M. Nasrallah, H.U. Anderson, D.M. Sparlin, and S.R. Sehlin, *Solid State Ionics*, **76**, 259 (1995).
11. L.W. Tai, M.M. Nasrallah, H.U. Anderson, D.M. Sparlin, and S.R. Sehlin, *Solid State Ionics*, **76**, 273 (1995).
12. M. Gödickemeier, K. Sasaki, L.J. Gaukler, and I. Riess, *Solid State Ionics*, **86**, 691 (1996).
13. M. Pillet, *Introduction aux plans d'expérience par la méthode Taguchi* (Éditions d'Organisation, 1992), p. 214.
14. D.S. McLachlan, M. Blaszkiewcz, and R.E. Newnham, *J. Amer. Ceram. Soc.*, **73**, 2187 (1990).
15. P.V. Dankwerts, *Appl. Sci. Res.* A, **3**, 279 (1953).
16. M. Coster and J.L. Chermant, *Précis d'analyse d'images* (Eds. du CNRS, 1989).
17. L.J. van der Pauw, *Philips Research Reports*, **13**, 1 (1958).
18. G.V. Samsonov, *The Oxide Handbook*, 2nd ed. (IFI/Plenum, New York, 1982), p. 419.
19. F.M. Figueiredo, J.A. Labrincha, J.R. Frade, and F.M.B. Marques, *Solid State Ionics*, **101**, 343 (1997).
20. F.M. Figueiredo, F.M.B. Marques, and J.R. Frade, *Solid State Ionics*, **138**, 173 (2001).
21. R. Walpole and R. Myers, *Probability and Statistics for Engineers and Scientists* (Collier MacMillan Int. Ed., New York, 1972).
22. M.W. Weiser, D.N. Lauben, P.G. Madrid, and K.B. Fong, *Ceram. Eng. Proc.*, **14**, 344 (1993).
23. H.D. Leigh and C.A. Towe, *Amer. Ceram. Soc. Bull.*, **66**, 786 (1987).